Flow and sound fields of temporal subsonic round jets

Christophe Bogey

Laboratoire de Mécanique des Fluides et d'Acoustique
UMR CNRS 5509, Ecole Centrale de Lyon
69134 Ecully Cedex, France
christophe.bogey@ec-lyon.fr

ABSTRACT

Two temporally-developing isothermal round jets at a Mach number of 0.9 and diameter-based Reynolds numbers Re_D of 3125 and 12500 are simulated in order to investigate their flow and acoustic fields. The simulations are carried out using high-order finite-difference schemes on a grid of 940 million points extending up to 120 jet radii in the axial direction. For each case, ten runs are performed, and their results are ensemble averaged. The jet at $\mathrm{Re}_D = 12500$ develops more rapidly, exhibits more fine turbulent scales, and generates more high-frequency acoustic waves than the jet at $\mathrm{Re}_D = 3125$. For both Reynolds numbers, however, a strong intermittency of the velocity field and high convection velocities are found on the jet axis at the time of the jet potential-core closing. At that time, low-frequency acoustic waves spaced by about 15 jet radii are also emitted in the downstream direction, as observed at the end of the potential core of spatially-developing jets. These results suggest the presence of the same sound source on the axis of temporally-developing and spatially-developing jets.

INTRODUCTION

In spite of more than fifty years of research, the mechanisms generating noise in subsonic jets are still not well understood (Tam, 1998). This is the case in particular for the sound source located at the end of the jet potential core, which appears to be responsible for a low-frequency noise component dominant in the downstream direction (Bogey *et al.*, 2003; Bogey & Bailly, 2007; Tam *et al.*, 2008). In order to characterize that sound source, it can be worth considering simplified models of the jet flow. Among the different possibilities, one consists in simulating temporally-developing jets. Temporal computations have been carried out in the past in many studies on fully-developed wall-bounded flows (Kim *et al.*, 1987; Eggels *et al.*, 1994; Kozul *et al.*, 2016) and mixing layers (Comte *et al.*, 1992; Freund *et al.*, 2000*a*,*b*; Fortuné *et al.*, 2004; Buchta & Freund, 2016). Applications to jets are however much less numerous (Hawkes *et al.*, 2007; van Reeuwijk & Holzner, 2014). Despite, or perhaps because of this, the simulations of temporal jets can be expected to provide new information on the physics of noise generation in subsonic jets.

In the present work, two temporally-developing isothermal round jets at a Mach number of 0.9 and diameter-based Reynolds numbers Re_D of 3125 and 12500 are simulated by solving the unsteady compressible Navier-Stokes equations using high-order numerical methods, in order to investigate the production of noise by such jets. The jet at the very low Reynolds number of $\mathrm{Re}_D = 3125$ was considered in a previous study (Bogey, 2017). The objective here is to describe the flow and acoustic fields of the two jets, and in particular to determine whether, for both Reynolds numbers, low-frequency acoustic waves are radiated when the jet mixing layers merge on the jet centerline, as happens at the end of the potential core of spatially-developing jets. If so, this will suggest that this noise component does not depend on the presence of a jet nozzle or of a potential core of finite length.

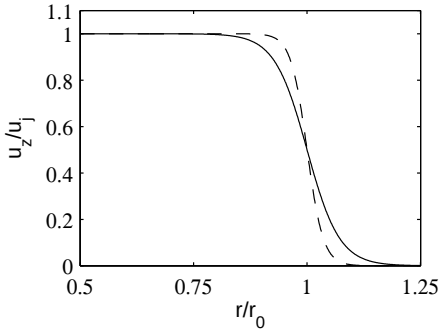

Figure 1. Radial profile of the axial velocity at $t = 0$ for ——— $\mathrm{Re}_D = 3125$ and − − − $\mathrm{Re}_D = 12500$.

The paper is organized as follow. The main parameters of the jets and of the simulations are first presented. Flow snapshots, and the main properties of the jet aerodynamic and acoustic fields are then provided. Finally, concluding remarks are given.

PARAMETERS

Jet Definition

The jets are isothermal, and have a Mach number of $\mathrm{M} = u_j/c = 0.9$ and Reynolds numbers of $\mathrm{Re}_D = u_j D/\nu = 3125$ and 12500, where u_j and $D = 2r_0$ are the jet initial centerline velocity and diameter, and c and ν are the speed of sound and kinematic molecular viscosity. At initial time $t = 0$, the axisymmetric mixing layers defined by the hyperbolic-tangent velocity profiles presented in figure 1 are considered. The momentum thicknesses of the mixing layers are set to $\delta_\theta = 0.0358 r_0$ and $0.0179 r_0$, respectively, following the variations of δ_θ/r_0 with the Reynolds number observed in experiments for initially laminar jets (Zaman, 1985).

At $t = 0$, velocity perturbations are added in the mixing layers in order to seed the laminar-turbulence transition. For this, ring vortices of radius r_0 and of random amplitude are imposed (Bogey *et al.*, 2003). These vortices have a half-width of $2\delta_\theta$, and are regularly distributed in the axial direction every $\Delta z = 0.025 r_0$. At each position, the vortex is weighted by the function associated with an azimuthal mode randomly chosen between 0 and 32. In this way, the initial peak turbulence intensity is about 1%, and ten runs are performed using different random seeds for each jet.

Numerical Methods

The simulations are carried out by solving the three-dimensional filtered compressible Navier-Stokes equations in cylindrical coordinates (r, θ, z) using low-dissipation and low-dispersion explicit schemes. In order to alleviate the time-step restriction near the cylindrical origin, the derivatives in the azimuthal direction around the axis are calculated at coarser resolutions than permitted by the grid (Mohseni & Colonius, 2000; Bogey *et al.*, 2011).

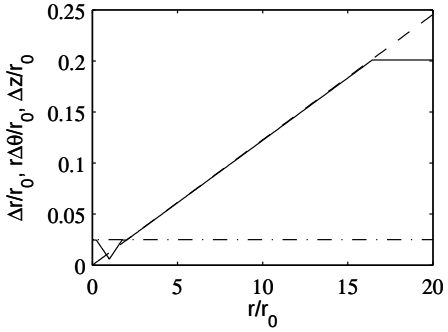

Figure 2. Radial profiles of the radial, azimuthal and axial mesh spacings ——— $\Delta r/r_0$, − − − $r\Delta\theta/r_0$ and − · − · $\Delta z/r_0$.

Fourth-order eleven-point centered finite differences are used for spatial discretization, and a second-order six-stage Runge-Kutta algorithm is implemented for time integration (Bogey & Bailly, 2004; Berland *et al.*, 2007). A twelfth-order thirteen-point centered filter is applied explicitly to the flow variables every time step in order to remove grid-to-grid oscillations. Radiation conditions are applied at the radial boundaries to avoid significant acoustic reflections (Tam & Dong, 1996; Bogey & Bailly, 2002), and periodic boundary conditions are imposed in the axial direction.

Simulation Parameters

The mesh grid extends up to $z = 120r_0$ in the axial direction, and out to $r = 30r_0$ in the radial direction. It contains $n_r = 382$, $n_\theta = 512$ and $n_z = 4800$ points. The mesh spacing in the axial direction is uniform and equal to $\Delta z = 0.025r_0$, whereas, as illustrated in figure 2, the mesh spacing in the radial direction varies. The latter is minimum and equal to $\Delta r = 0.006r_0$ at $r = r_0$. It is maximum and equal to $\Delta r = 0.2r_0$ for $r \geq 16r_0$, yielding a Strouhal number of $\mathrm{St}_D = 2.8$ for an acoustic wave discretized by four points per wavelength. Finally, the use of $n_\theta = 512$ points in the azimuthal direction leads to $r\Delta\theta = 0.012r_0$ at $r = r_0$.

The computations are performed using an OpenMP-based in-house solver. For each run, the total number of iterations is equal to 23,000 for $\mathrm{Re}_D = 3125$ and 14,000 for $\mathrm{Re}_D = 12500$, yielding a final time of $t = 75r_0/u_j$. For the present grid of about one billion points, 200 GB of memory are required, and about 1,000 CPU hours are consumed for 1,000 iterations. Density, the three velocity components, pressure and vorticity norm are recorded on the jet axis at $r = 0$ and on the cylindrical surfaces at $r = r_0$, $4r_0$ and $20r_0$, at a sampling frequency allowing spectra to be computed up to $\mathrm{St}_D = 10$, and on the four azimuthal planes at $\theta = 0$, $\pi/2$, π and $3\pi/2$, at half the frequency mentioned above. The statistical results obtained in each run are averaged over the directions z and θ. The results of the ten runs are then ensemble averaged.

RESULTS

Snapshots

Snapshots of the vorticity norm and pressure fluctuations obtained in the (z,r) plane for $\mathrm{Re}_D = 3125$ at times $t^\star = tu_j/r_0 = 20$ and $t^\star = 40$ and for $\mathrm{Re}_D = 12500$ at $t^\star = 15$ and $t^\star = 35$ are represented in figures 3 and 4, respectively. For both Reynolds numbers, two turbulent mixing layers can be seen on both sides of the jet axis in the top figure, and they have merged in the bottom figure. More fine turbulent scales are observed in the higher Reynolds number case, as expected.

In the pressure fields of the jet at $\mathrm{Re}_D = 3125$, in figure 3, alternatively positive and negative fluctuations are found in the close vicinity of the jet at $t^\star = 20$. They are most likely the footprints of the large turbulent structures of the jet in the pressure near field. At time $t^\star = 40$, after the potential-core closing, high-amplitude waves, with a typical wavelength of about $15r_0$, appear to propagate in the downstream direction. They look like the waves emitted at shallow angles by spatially-developing subsonic jets (Bogey & Bailly, 2006). For $\mathrm{Re}_D = 12500$, in figure 4, after a strong initial acoustic component due to the shear-layer rolling-up, sound waves with various wavelengths radiate in the pressure field. The downstream-propagating low-frequency waves mentioned above for $\mathrm{Re}_D = 3125$ are also noticeable at $t^\star = 35$. Upstream-propagating high-frequency waves can also be detected in this case.

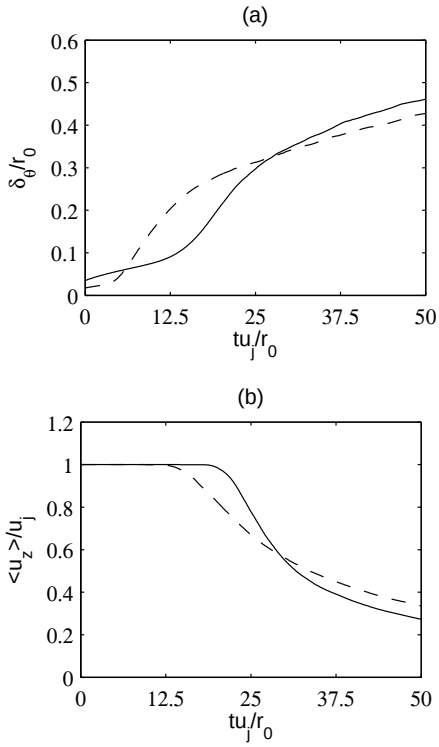

Figure 5. Time variations of (a) the shear-layer momentum thickness and (b) the mean axial velocity at $r = 0$ for ——— $\mathrm{Re}_D = 3125$ and − − − $\mathrm{Re}_D = 12500$.

Flow Fields

The time variations of the shear-layer momentum thickness and of the mean centerline axial velocity are presented in figure 5. The shear-layer spreading and jet development start earlier for $\mathrm{Re}_D = 12500$ than for $\mathrm{Re}_D = 3125$, leading to the mean centerline velocity of $0.95u_j$ at $tu_j/r_0 = 16$ in the former case, but at $tu_j/r_0 = 21.6$ in the latter. Then, they occur more slowly in the higher Reynolds number case.

The time variations of the rms values and of the skewness and kurtosis factors of axial velocity fluctuations at $r = 0$ and $r = r_0$ are displayed in figure 6. In figure 6(a), strong humps are obtained in the profiles of turbulence intensity, leading to maximum values of 17% at $r = 0$ and 20% at $r = r_0$ for $\mathrm{Re}_D = 3125$, and of 12.6% at $r = 0$ and 21.3% at at $r = r_0$ for $\mathrm{Re}_D = 12500$. As expected, due to the difference in mean flow development, they are reached much earlier in the $\mathrm{Re}_D = 12500$ case. They result from the mergings of vortical structures (Bogey & Bailly, 2010) in the shear layers and on the jet centerline, respectively. In figures 6(b) and 6(c), values of skewness around -1.1 and values of kurtosis higher than 6 are found at $r = 0$ close to the time of potential-core closing for

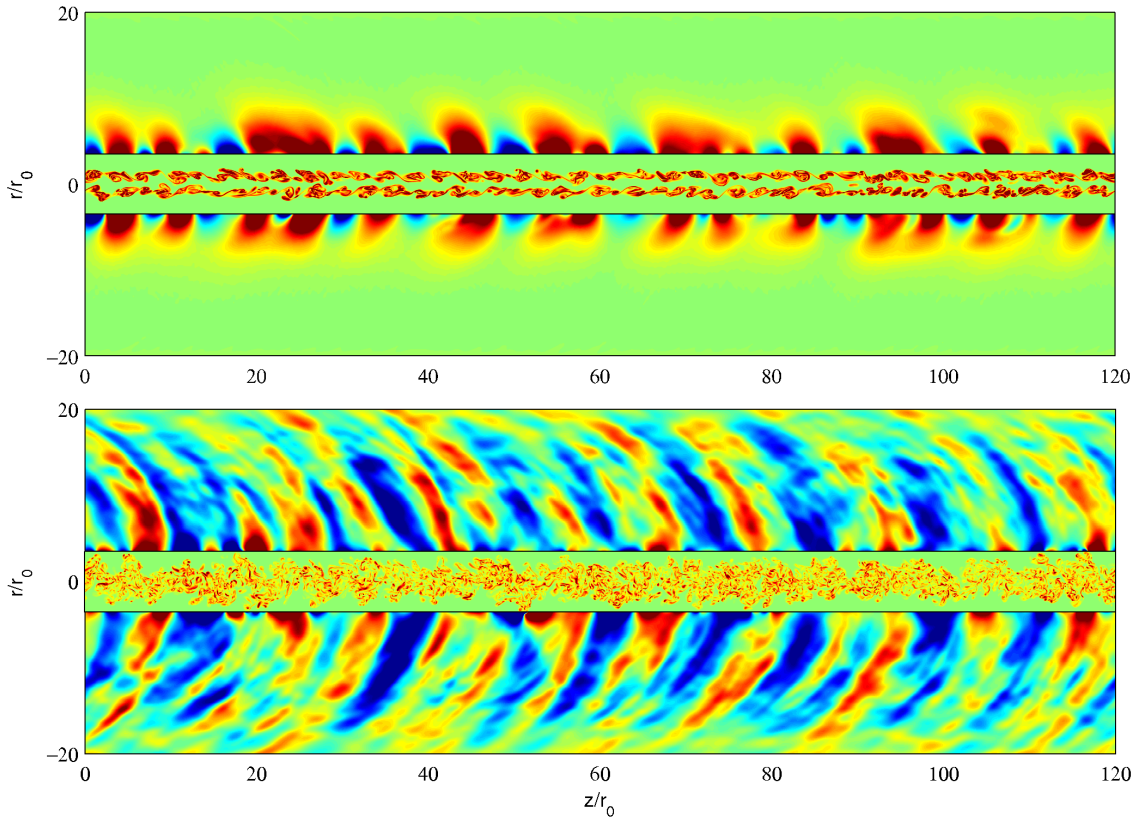

Figure 3. Vorticity and pressure fluctuations obtained for $\mathrm{Re}_D = 3125$ at $tu_j/r_0 = 20$ and 40, from top to bottom. The color scales range up to the level of $4u_j/r_0$ for vorticity, and from -200 Pa to 200 Pa for pressure.

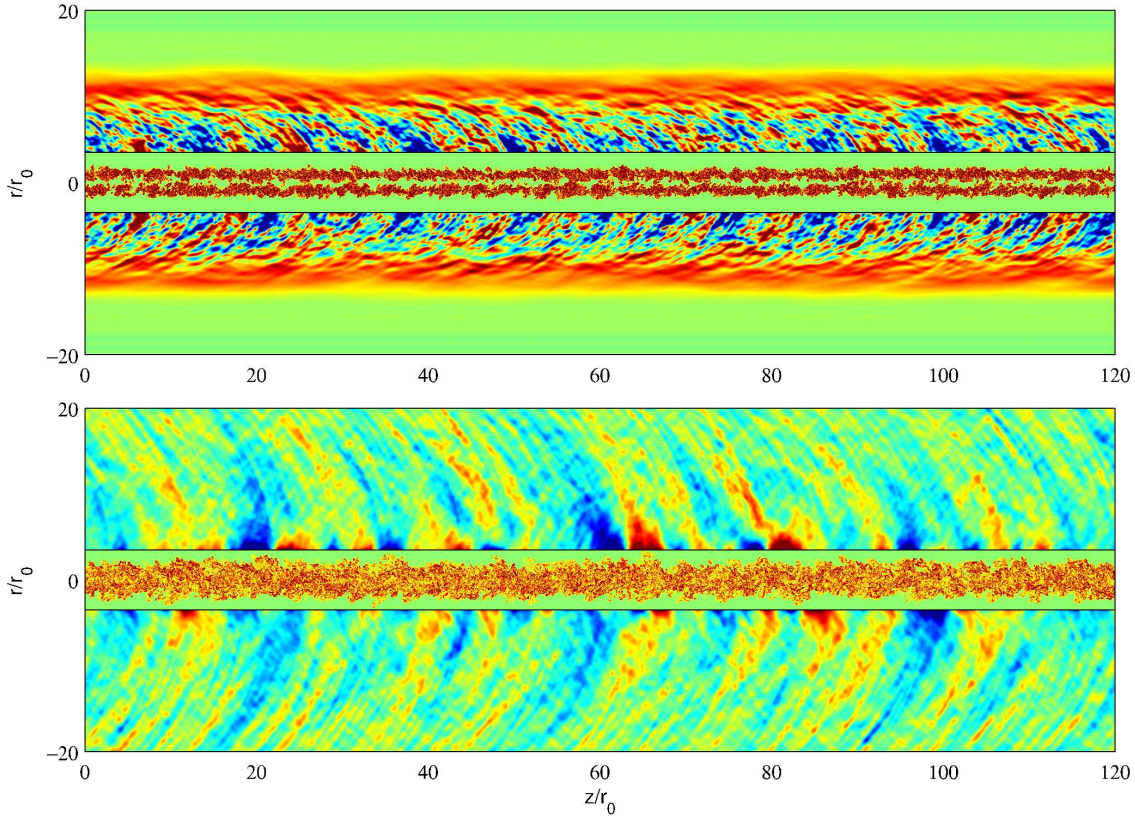

Figure 4. Vorticity and pressure fluctuations obtained for $\mathrm{Re}_D = 12500$ at $tu_j/r_0 = 15$ and 35, from top to bottom. The color scales range up to the level of $4u_j/r_0$ for vorticity, and from -200 Pa to 200 Pa for pressure.

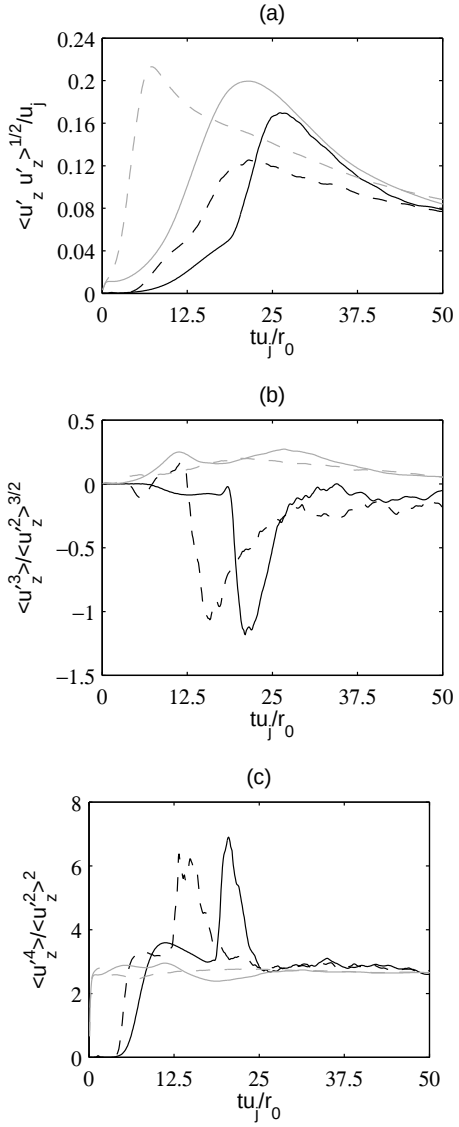

Figure 6. Time variations of (a) the rms values and (b) the skewness and (c) the kurtosis factors of the axial velocity fluctuations at $r = 0$ for ——— $\mathrm{Re}_D = 3125$ and − − − $\mathrm{Re}_D = 12500$, and at $r = r_0$ for ——— $\mathrm{Re}_D = 3125$ and − − − $\mathrm{Re}_D = 12500$.

both Reynolds numbers. This indicates intermittent occurrence of velocity deficits on the jet centerline at that time. They very probably follow the intrusion of shear-layer turbulent structures in the potential core of the temporal jet, as it happens at the end of the potential core of spatially-developing jets (Bogey *et al.*, 2003; Bogey & Bailly, 2007). At $r = r_0$, the kurtosis factor does not deviate appreciably from the value of 3, but the skewness factor is slightly positive, suggesting possible bursts of high-velocity flow structures in the mixing layers.

The convection velocities of the flow structures obtained at $r = 0$ and at $r = r_0$ from correlations of axial velocity fluctuations are represented in figure 7 as a function of time. On the jet axis, the convection velocity reaches a peak value of $0.86u_j$ for $\mathrm{Re}_D = 3125$ and of $0.95u_j$ for $\mathrm{Re}_D = 12500$ near the time of potential-core closing. This implies that that the turbulent structures that enter into the potential core are accelerated, as in spatially-developing jets (Bogey & Bailly, 2007). At $r = r_0$, on the contrary, the convection velocity decreases monotonically.

The spectra of axial velocity fluctuations evaluated at $r = 0$

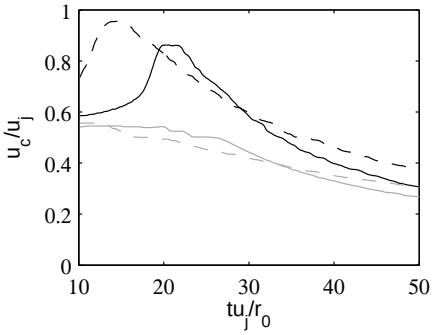

Figure 7. Time variations of the convection velocity obtained at $r = 0$ for ——— $\mathrm{Re}_D = 3125$ and − − − $\mathrm{Re}_D = 12500$, and at $r = r_0$ for ——— $\mathrm{Re}_D = 3125$ and − − − $\mathrm{Re}_D = 12500$.

and at $r = r_0$ for $\mathrm{Re}_D = 3125$ are presented in figure 8 as functions of axial wavenumber k_z and time. That obtained at $r = r_0$ for $\mathrm{Re}_D = 12500$ is shown in figure 9. In figure 8(a), the spectrum on the jet axis, though poorly converged, exhibits at $tu_j/r_0 = 24$ peak levels around a wavenumber $k_z r_0 \simeq 0.4$, yielding a spatial wavelength $\lambda_z \simeq 15r_0$. This spatial periodicity roughly corresponds to that observed in the pressure fields of figure 3. In figure 8(b) and figure 9, the spectra at $r = r_0$ are much better converged, and exhibit more high-frequency components, than that at $r = 0$. Moreover, the spectrum for $\mathrm{Re}_D = 12500$ is more broadband than that for $\mathrm{Re}_D = 3125$.

Acoustic Fields

The time variations of the rms values and of the skewness and kurtosis factors of the pressure fluctuations at $r = 10r_0$ are represented in figure 10. In figure 10(a), the rms pressure profiles reach maximum values of 83 Pa at $tu_j/r_0 = 35.4$ for $\mathrm{Re}_D = 3125$ and of 68 Pa at $tu_j/r_0 = 19$ for $\mathrm{Re}_D = 12500$. Given the times of potential-core closing, equal to $tu_j/r_0 = 21.6$ in the former case and to $tu_j/r_0 = 16$ in the latter, the peak for $\mathrm{Re}_D = 3125$ may be due to the merging of turbulent structures on the jet axis, but it cannot for $\mathrm{Re}_D = 12500$. In that case, it may result from vortex pairings in the shear layers. As for the skewness factor in figure 10(b) and the kurtosis factor in figure 10(c), significant positive values and values different from 3 are respectively found at the early growth stages of the acoustic levels. Later, they are close to 0 and 3, indicating that non-linear effects and intermittency are negligible in the near fields of the jets.

The spectra of pressure fluctuations calculated at $r = 10r_0$ for $\mathrm{Re}_D = 3125$ are presented in figure 11 as functions of axial wavenumber k_z and time. Those obtained at $r = 5r_0$, $r = 10r_0$ and $r = 20r_0$ for $\mathrm{Re}_D = 12500$ are displayed in figure 12. For both Reynolds numbers, whatever the position, a band of high levels emerges around a wavenumber $k_z r_0 \simeq 0.4$. This band extends over a long time period, e.g. between $tu_j/r_0 = 25$ and $tu_j/r_0 = 60$ in figure 12(b), and can be related to the presence of sound waves of wavelength of $\lambda_z \simeq 15r_0$ in the pressure fields of figure 3. Since strong components are also found around $k_z r_0 \simeq 0.4$ in the spectrum of centerline velocity of figure 8(a) just after the time of potential-core closing, these waves are very likely to be generated when the jet mixing layers merge on the axis.

CONCLUSION

In this paper, the flow and acoustic fields obtained for two temporally-developing isothermal round jets at a Mach number of 0.9 and Reynold numbers of 3125 and 12500 are presented. The difference in Reynolds number leads to a more rapid flow develop-

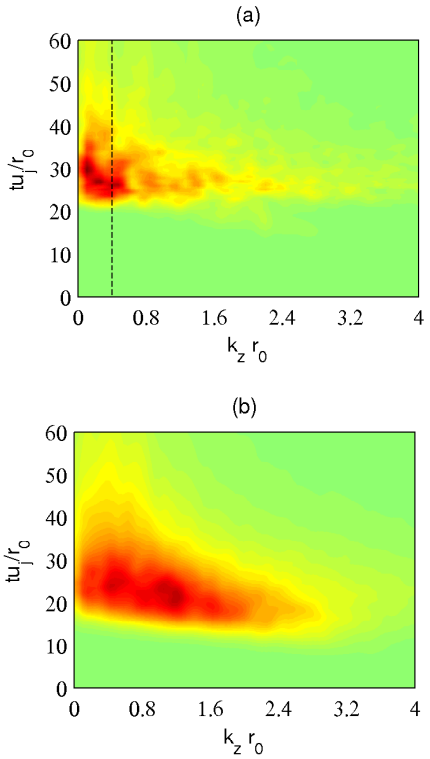

Figure 8. Representation of the power spectral densities of the axial velocity fluctuations obtained at (a) $r = 0$ and (b) $r = r_0$ for $\mathrm{Re}_D = 3125$ as a function of axial wavenumber, using the colorbar levels in the two figures; – – – $k_z r_0 = 0.4$.

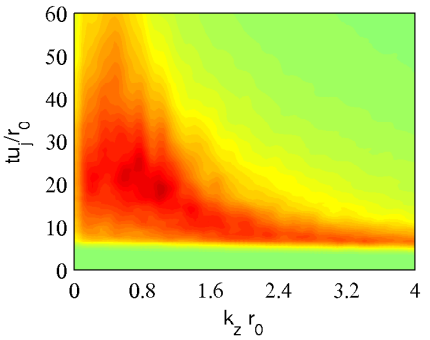

Figure 9. Representation of the power spectral densities of the axial velocity fluctuations obtained at $r = r_0$ for $\mathrm{Re}_D = 12500$ as a function of axial wavenumber; – – – $k_z r_0 = 0.4$. The colorbar levels are 1.8 times lower than those in figure 8.

ment and more broadband velocity and pressure spectra for the jet at $\mathrm{Re}_D = 12500$. Despite this, in both cases, the merging of the mixing layers results in significant intermittency and high convection velocity on the jet axis, and appears to produce low-frequency sound waves radiating in the downstream direction. This behaviour is very similar to that observed at the end of the potential core of spatially-developing jets, suggesting the presence of the same sound source on the axis of temporally-developing and spatially-developing jets.

ACKNOWLEDGMENTS

This work was granted access to the HPC resources of FLMSN (Fédération Lyonnaise de Modélisation et Sciences Numériques), partner of EQUIPEX EQUIP@MESO, and of the resources of CINES (Centre Informatique National de l'Enseignement Supérieur) and IDRIS (Institut du Développement et des Ressources en Informatique Scientifique) under the allocation 2016-2a0204 made by GENCI (Grand Equipement National de Calcul Intensif). It was performed within the framework of the Labex CeLyA of Université de Lyon, operated by the French National Research Agency (Grant No. ANR-10-LABX-0060/ANR-11-IDEX-0007).

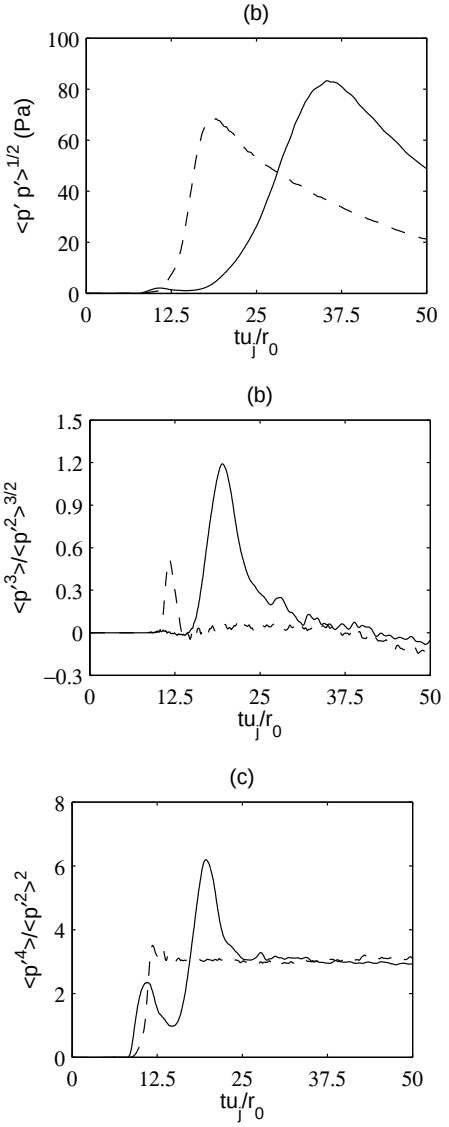

Figure 10. Time variations of (a) the rms values and (b) the skewness and (c) the kurtosis factors of the pressure fluctuations at $r = 10r_0$ for ——— $\mathrm{Re}_D = 3125$ and – – – $\mathrm{Re}_D = 12500$.

REFERENCES

Berland, J., Bogey, C., Marsden, O. & Bailly, C. 2007 High-order, low dispersive and low dissipative explicit schemes for multi-scale and boundary problems. *J. Comput. Phys.* **224** (2), 637–662.

Bogey, C. 2017 Direct numerical simulation of a temporally-developing subsonic round jet and its sound field. *AIAA Paper 2017-0925* .

Bogey, C. & Bailly, C. 2002 Three-dimensional non reflective boundary conditions for acoustic simulations: far-field formulation and validation test cases. *Acta Acustica* **88** (4), 463–471.

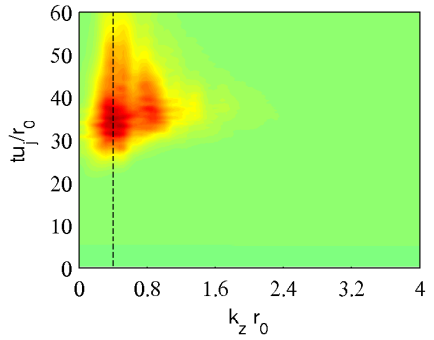

Figure 11. Representation of the power spectral densities of pressure fluctuations obtained for $\mathrm{Re}_D = 3125$ at $r = 10r_0$, as a function of axial wavenumber.

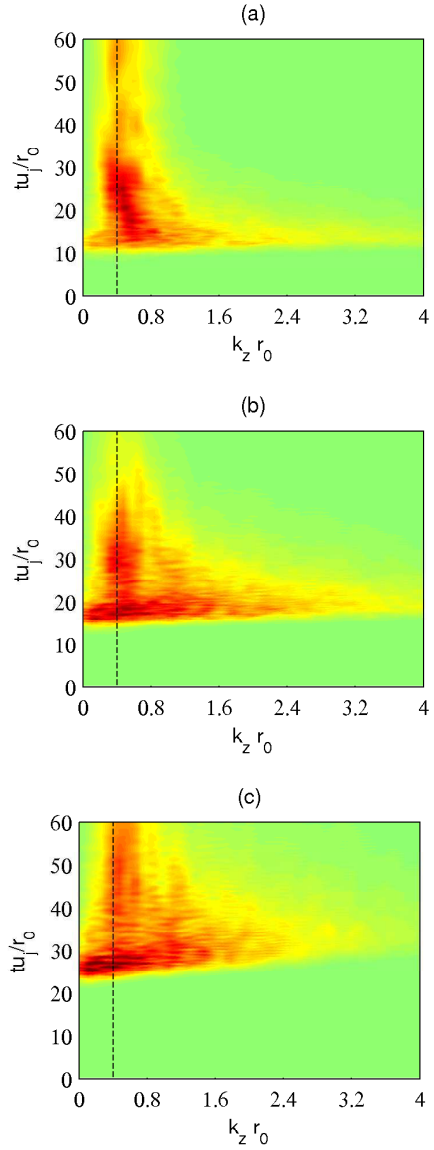

Figure 12. Representation of the power spectral densities of pressure fluctuations obtained for $\mathrm{Re}_D = 12500$ at (a) $r = 5r_0$, (b) $r = 10r_0$ and (c) $r = 20r_0$, as a function of axial wavenumber; $- - -$ $k_z r_0 = 0.4$.

Bogey, C. & Bailly, C. 2004 A family of low dispersive and low dissipative explicit schemes for flow and noise computations. *J. Comput. Phys.* **194** (1), 194–214.

Bogey, C. & Bailly, C. 2006 Investigation of downstream and sideline subsonic jet noise using large eddy simulations. *Theor. Comput. Fluid Dyn.* **20** (1), 23–40.

Bogey, C. & Bailly, C. 2007 An analysis of the correlations between the turbulent flow and the sound pressure field of subsonic jets. *J. Fluid Mech.* **583**, 71–97.

Bogey, C. & Bailly, C. 2010 Influence of nozzle-exit boundary-layer conditions on the flow and acoustic fields of initially laminar jets. *J. Fluid Mech.* **663**, 507–539.

Bogey, C., Bailly, C. & Juvé, D. 2003 Noise investigation of a high subsonic, moderate reynolds number jet using a compressible les. *Theor. Comput. Fluid Dyn.* **16** (4), 273–297.

Bogey, C., de Cacqueray, N. & Bailly, C. 2011 Finite differences for coarse azimuthal discretization and for reduction of effective resolution near origin of cylindrical flow equations. *J. Comput. Phys.* **230** (4), 1134–1146.

Buchta, D.A. & Freund, J.B. 2016 The role of large-scale structures on crackle noise. *AIAA Paper 2016-3027* .

Comte, P., Lesieur, M. & Lamballais, E. 1992 Large- and small-scale stirring of vorticity and a passive scalar in a 3-d temporal mixing layer. *Phys. Fluids A* **4** (12), 2761–2778.

Eggels, J.G.M., Unger, F., Weiss, M.H., Westerweel, J., Adrian, R.J., Friedrich, R. & Nieustadt, F.T.M. 1994 Fully developed turbulent pipe flow: a comparison between direct numerical simulation and experiment. *J. Fluid Mech.* **268**, 175–209.

Fortuné, V., Lamballais, E. & Gervais, Y. 2004 Noise radiated by a non-isothermal, temporal mixing layer. part i: Direct computation and prediction using compressible dns. *Theor. Comput. Fluid Dyn.* **18** (1), 61–81.

Freund, J.B., Lele, S.K. & Moin, P. 2000*a* Compressibility effects in a turbulent annular mixing layer. part 1. turbulence and growth rate. *J. Fluid Mech.* **421**, 229–267.

Freund, J.B., Lele, S.K. & Moin, P. 2000*b* Compressibility effects in a turbulent annular mixing layer. part 2. mixing of a passive scalar. *J. Fluid Mech.* **421**, 269–292.

Hawkes, E.R., Sankaran, R., Sutherland, J.C. & Chen, J.H. 2007 Scalar mixing in direct numerical simulations of temporally evolving plane jet flames with skeletal co/h_2 kinetics. *Proc. Combust. Inst.* **31** (1), 1633–1640.

Kim, J., Moin, P. & Moser, R. 1987 Turbulence statistics in fully developed channel flow at low reynolds number. *J. Fluid Mech.* **177**, 133–166.

Kozul, M., Chung, D. & Monty, J.P. 2016 Direct numerical simulation of the incompressible temporally developing turbulent boundary layer. *J. Fluid Mech.* **796**, 437–472.

Mohseni, K. & Colonius, T. 2000 Numerical treatment of polar coordinate singularities. *J. Comput. Phys.* **157** (2), 787–795.

van Reeuwijk, M. & Holzner, M. 2014 The turbulence boundary of a temporal jet. *J. Fluid Mech.* **739**, 254–275.

Tam, C.K.W. 1998 Jet noise: since 1952. *Theor. Comput. Fluid Dyn.* **10**, 393–405.

Tam, C.K.W & Dong, Z. 1996 Radiation and outflow boundary conditions for direct computation of acoustic and flow disturbances in a nonuniform mean flow. *J. Comput. Acoust.* **4** (2), 175–201.

Tam, C.K.W., Viswanathan, K., Ahuja, K.K. & Panda, J. 2008 The sources of jet noise: experimental evidence. *J. Fluid Mech.* **615**, 253–292.

Zaman, K.B.M.Q. 1985 Effect of initial condition on subsonic jet noise. *AIAA J.* **23** (9), 1370–1373.